Hindawi
Geofluids
Volume 2021, Article ID 6641419, 9 pages
https://doi.org/10.1155/2021/6641419

Research Article

Microstructural Features of Freezing and Thawing-Creep Damages for Concrete Mixed with Fly Ash

Bing Li,[1] **Lian-ying Zhang**,[1] **Ming Li**,[2] **Hai Pu**,[2] **Chao Ma**,[1] **and Pei-tao Qiu**[1]

[1]*School of Civil Engineering, Xuzhou Institute of Technology, Xuzhou, 221008 Jiangsu, China*
[2]*State Key Laboratory of Geomechanics and Deep Underground Engineering, China University of Mining & Technology, Xuzhou, 221008 Jiangsu, China*

Correspondence should be addressed to Lian-ying Zhang; zhanglianying@126.com

Received 10 November 2020; Revised 30 December 2020; Accepted 26 February 2021; Published 12 March 2021

Academic Editor: Huazhou Li

The macroscopic morphology characteristics, pore structure characteristics, and microfracture morphology of concrete with fly ash subjected to the freeze-thaw-creep effect were analyzed via scanning electron microscopy (SEM). The results revealed that the macrosection of a specimen subjected to freeze-thaw cycling evolves from a regular to an irregular morphology in which the degree of fragmentation increases. Four specimen pore structure types characterized by single holes, nonconnected hole clusters, connected hole clusters, and fly ash holes, respectively, were identified. The microfracture morphology of the concrete was found to include five types of brittle fractures—river, step, cascade, hemispherical, and irregular patterns—and two types of ductile fractures—dimple and peak forest patterns. Two sets of experiments in which (1) the fly ash content ($m = 35\%$) was kept constant and the number of freeze-thaw cycles increased, and (2) the number of freeze-thaw cycles ($n = 120$) was kept constant, and the fly ash content was increased were carried out. In both cases, the number of connected hole clusters increased and a surrounding skeleton structure with a needle filamentous or flaky appearance was produced. In addition, the degree of deterioration of the pore structure increased and the fracture features changed from brittle to ductile.

1. Introduction

The deeper underground space is a complicated environment associated with high ground stress, high ground temperature, and high karst water pressure, which poses significant challenges to engineering personnel and scientific researchers [1–5]. Concrete is one of the most widely used building materials, where applications have extended beyond conventional buildings to underground, aquatic, and marine structures. Concrete materials can incur damage as a result of environmental factors such as high and low temperatures, high pressure, corrosion, wind load, freezing and thawing, and rain and snow. Such factors can produce deformations in engineering structures and can eventually lead to structural instability. Accordingly, the physical-mechanical response of concrete materials and structures under one or more factor conditions has become a subject of intense research in the fields of building materials and structural engineering [6, 7]. Numerous studies have looked at the property changes and damage mechanisms of concretes in freezing and thawing environments [8, 9], leading to a number of techniques for improving the antifreezing and thawing properties of these materials. However, many problems must still be resolved, including the physical-mechanical behaviors [10, 11], damage mechanisms [12, 13], and micromechanical behaviors [14, 15] of different concrete materials (high-strength, high-performance, very-high performance, fiber concrete, etc.) under the coupling of freezing and thawing and other factors (load, corrosion, etc.).

With the continuous increase in energy demand, mineral resources extraction has gradually shifted to deeper strata, and the development depth of vertical shafts has increased consequently, along with the increase in the cross-sectional size of the shaft [16–18]. For the development of deep and thick unstable aquifer mines, the artificial ground freezing method is widely used [19–21]. When constructing using the freezing method, the freezing shaft lining is crucial, and its main function is to block groundwater and withstand

Table 1: Chemical composition of cement.

Materials	SiO_2	Al_2O_3	Fe_2O_3	CaO	MgO	Na_2O	K_2O	SO_3
Cement	21.60%	4.13%	4.57%	64.44%	1.06%	0.11%	0.56%	1.74%
Fly ash	54.90%	25.80%	6.90%	8.70%	1.80%	0.30%	0.10%	0.60%

Table 2: Mix ratio of concrete.

Fly ash content m/%	Fly ash kg/m^3	Cement kg/m^3	Sand kg/m^3	Stone kg/m^3	Water-cement ratio	Water kg/m^3
0.0	0.0	453.0	740.0	1112.0	0.32	145.0
20.0	91.0	362.0	740.0	1112.0	0.32	145.0
35.0	159.0	294.0	740.0	1112.0	0.32	145.0
50.0	226.5	226.5	740.0	1112.0	0.32	145.0

the temporary load to ensure the safety and smooth operation of shaft sinking construction [22–25]. The structural forms of freezing shaft lining primarily include single-layer reinforced concrete, double-layer reinforced concrete, and reinforced concrete composite shaft lining. Currently, concrete materials are essential in the construction of all freezing shaft lining.

Rheology, which must always be taken into consideration in the design and construction of concrete engineering structures, is one of the more important factors determining the degree of failure and damage experienced by concrete engineering structures after long-term service. Accordingly, there has been a significant amount of research on the rheological properties of concrete materials and structures [26–28]. Understanding the creep deformation features and the microstructural change laws of concrete materials under freezing and thawing conditions plays a critical role in improving the freezing and thawing resistance and durability of concretes.

Analysis of the microcomponents and morphological structures of materials is the key to understanding their mechanical properties and damage mechanisms [29]. Based on preliminary research [30–32] and the scanning electron microscope, the overall morphology and structural features of the micropores and microtopographic features of concrete mixed with fly ash by the freezing and thawing-creep action were studied. The results constitute a foundation for understanding the micromechanical mechanisms of the damage fracturing for concrete mixed with fly ash by the freezing and thawing-creep action.

2. Test Method

2.1. Materials. The cementitious materials used in the experiment were Portland cement and fly ash (FA) supplied by two local companies. The chemical components of these materials are listed in Table 1. River sand with a fineness modulus of 2.8 and an apparent density of 2,769 kg/m^3 was used as a fine aggregate; crushed limestone with a size of 5–20 mm and an apparent density of 2,719 kg/m^3 was used as a coarse aggregate. Carboxylic acid provided by Zhejiang Wulong Chemical Co. Ltd was used as a slushing agent for the concrete. The mix proportions used in the concrete are summarized in Table 2.

2.2. Test Method. Concrete specimens were subjected to freezing and thawing-creep deformation testing. Each specimen had the dimensions $100 \times 100 \times 300$ mm^3 and had been subjected to curing for more than 90 d. There were three specimens in each group. The uniaxial compressive strength of cube concrete specimens ($100 \times 100 \times 100$ mm^3) with different fly ash replacement ratios were 58.1 MPa ($m = 0\%$), 65.5 MPa ($m = 20\%$), 63.4 MPa ($m = 35\%$), and 53.8 MPa ($m = 50\%$).

After each set of 30 rapid freezing-and-thawing cycles (GBT50082-2009 China), the specimens were subjected to creep deformation testing. A Changchun Kexin YAS-5000 microprocessor-controlled electro-hydraulic servo compression-testing machine was used to carry out creep deformation tests under progressive loading. Each specimen was first loaded to 30% of its strength value at a loading rate of 2 kN/s, after which the loading was maintained at the strain stability state. Following this, the load value was progressively increased by 10% of the uniaxial compressive strength, with the loading maintained at the strain stability state, until the specimen was damaged. The testing units used for the creep deformation testing are shown in Figure 1.

SEM testing was then applied to the concrete specimen fragments. The testing units for the SEM analysis are shown in Figure 2. The serial no. of the SEM test system is TESCAN VGEA3 provided by the Civil Structure Laboratory of Xuzhou Institute of Engineering.

3. Results and Discussion

3.1. Macro Features of Creep Fractures of Fly Ash Concretes after Freezing and Thawing. Figure 3 shows the macrofracture features of concrete specimens with fly ash replacements of $m = 0$, 20, 35, and 50% and following $n = 0$, 30, 60, 90, and 120 freezing-and-thawing cycles (magnification 15x).

The macrofractures of the specimens evolved from a smooth to a concave-convex irregular morphology as the

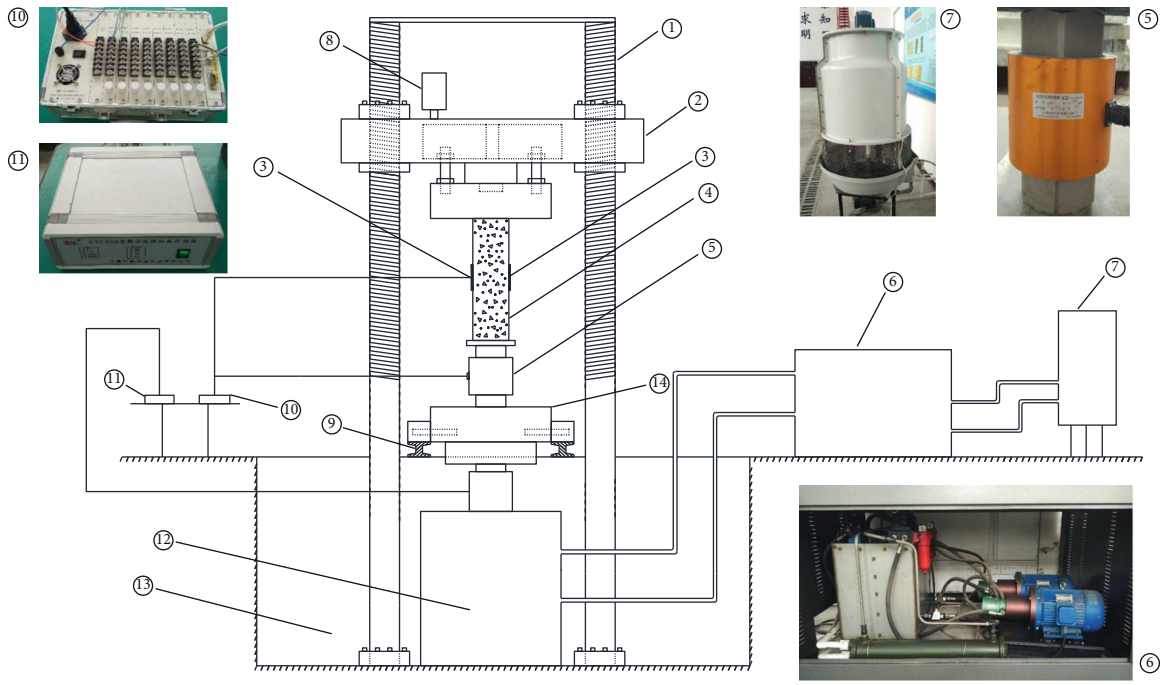

Figure 1: Electrohydraulic servo creep test system: ① Guide screw. ② Bearing plate. ③ Strain gauge. ④ Concrete. ⑤ Pressure transducer. ⑥ Oil pump system. ⑦ Cooling tower. ⑧ Electric machinery. ⑨ Track. ⑩ Strain collection device. ⑪ Controller. ⑫ Power device. ⑬ Underground space. ⑭ Bearing plate.

Figure 2: Scanning electron microscope used in SEM analysis.

number of freezing-and-thawing cycles increased. As the number of fractures per section increased, the specimens were progressively divided into many small regions. For example, the sample with a fly ash replacement of $m = 0\%$ (Figures 3(a)–3(e)) had a relatively smooth fracture surface and relatively favorable integrity following $n = 0$ and 30 cycles of freezing and thawing; after $n = 60$, 90, and 120 cycles, however, the specimen developed an unsmooth fracture surface with unfavorable integrity.

The postfreezing-and-thawing fly ash concrete specimens experienced more deterioration in fracture surface smoothness and integrity than did the specimens with no

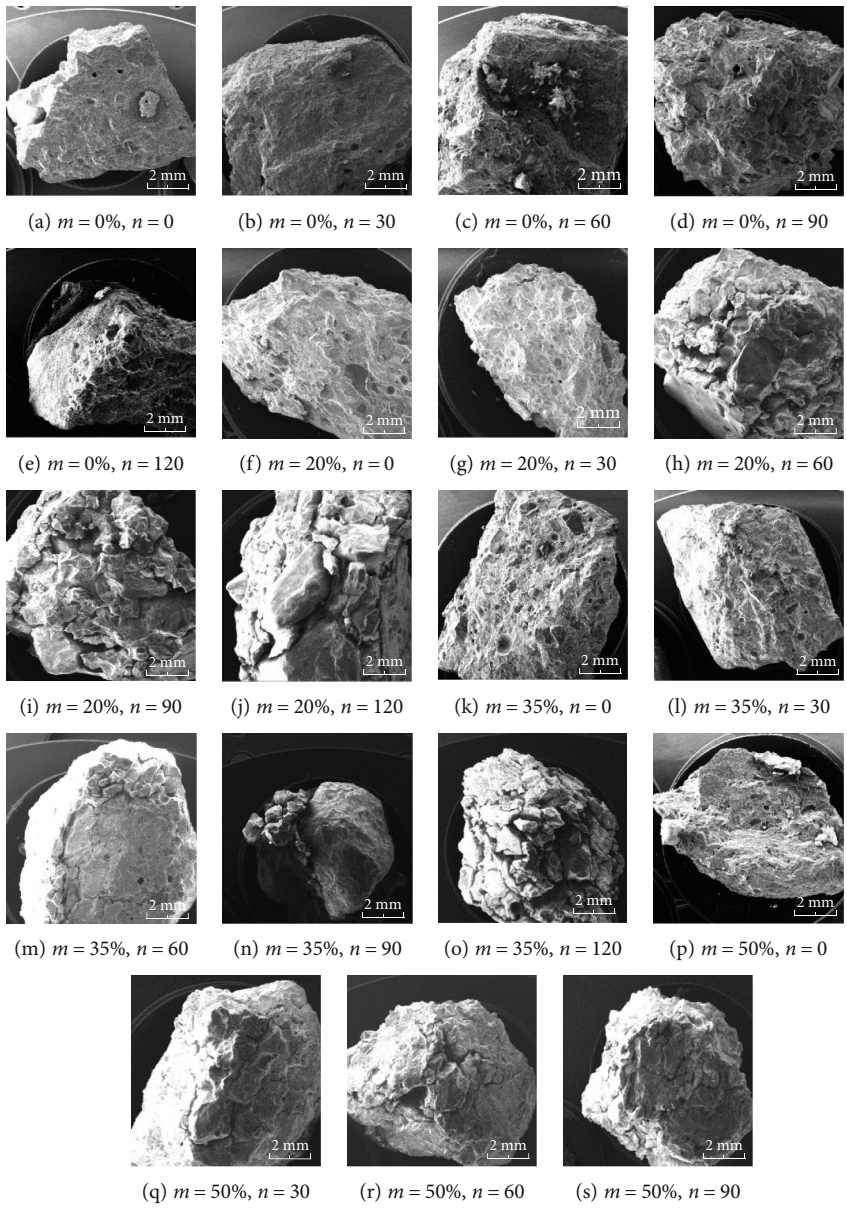

(a) $m = 0\%$, $n = 0$ (b) $m = 0\%$, $n = 30$ (c) $m = 0\%$, $n = 60$ (d) $m = 0\%$, $n = 90$

(e) $m = 0\%$, $n = 120$ (f) $m = 20\%$, $n = 0$ (g) $m = 20\%$, $n = 30$ (h) $m = 20\%$, $n = 60$

(i) $m = 20\%$, $n = 90$ (j) $m = 20\%$, $n = 120$ (k) $m = 35\%$, $n = 0$ (l) $m = 35\%$, $n = 30$

(m) $m = 35\%$, $n = 60$ (n) $m = 35\%$, $n = 90$ (o) $m = 35\%$, $n = 120$ (p) $m = 50\%$, $n = 0$

(q) $m = 50\%$, $n = 30$ (r) $m = 50\%$, $n = 60$ (s) $m = 50\%$, $n = 90$

Figure 3: Macroscopic failure characteristics of concrete after freeze-thaw cycling and creep.

fly ash, with the degree of deterioration increasing with the percentage of fly ash replacement. For example, the $m = 0$ and 20% specimens had relatively smooth fracture surfaces with favorable integrity after $n = 30$ cycles (Figures 3(b) and 3(g), respectively), whereas the $m = 35\%$ specimen had a relatively rougher fracture surface and unfavorable integrity (Figure 3(l)) and the $m = 50\%$ specimen had an irregular fracture surface, large amounts of fracturing, and even worse integrity (Figure 3(q)).

3.2. Pore Structure Features of Fly Ash Concrete after Freezing and Thawing-Creep Deformation. The size, quantity, and distribution of pores in a concrete have a direct effect on its physical and mechanical properties. Previous research has shown that the pore structure features of a concrete are closely related to its antifrost properties [33]. Based on SEM observation and analysis of the pore structure features of the fly ash concrete specimens following freezing and thawing and creep deformation, the following four types of pore structure were identified:

Single-pore: in these structures, individual air bubbles remained in the cement paste and failed to escape during the concrete hardening process, resulting in the formation of single pores that were distributed within the specimen in a dispersive manner, as shown in Figure 4(a).

Disconnected pore clusters: in these structures, multiple concentrations of air bubbles remained in the cement paste during the concrete hardening process (alternatively, large air bubbles were deformed or divided as a result of extrusion of cement paste), resulting in the formation of pore clusters, as shown in Figure 4(b).

Connected pore clusters: during the concrete hydration process, products can fill and obstruct large pores, resulting

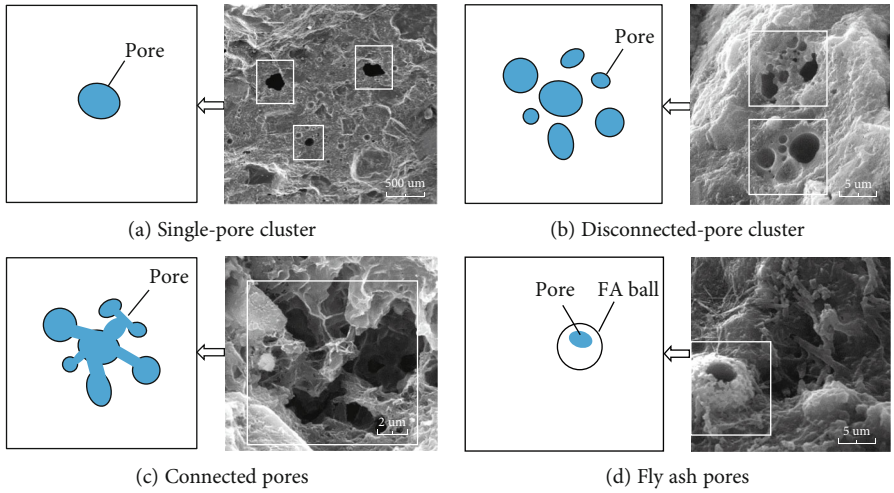

Figure 4: Pore characteristics of concrete mixed with fly ash after freezing-thawing cycles and creep.

in the formation of connected pore clusters. Alternatively, disconnected pore clusters can incur damage to their pore walls as a result of external environmental effects such as freezing and thawing or corrosion, resulting in the formation of connected pore clusters, as shown in Figure 4(c). The presence of honeycomb-type connected pore clusters has a detrimental effect on the mechanical properties of concrete materials.

Fly ash (FA) pores: although most fly ash ball particles are solid particles, some are hollow or semi-hollow. Pores can be generated when the surfaces of such ball particles are fractured, as shown in Figure 4(d).

To further analyze the influence of freezing and thawing on concrete pore structure features, SEM images of concretes ($m = 35\%$) following different numbers of freezing-and-thawing cycles were analyzed (Figure 5, magnification 5000x). The number of harmful pores with diameters in the range of 200–5,000 nm increased with the number of freezing-and-thawing cycles, leading to loosened frameworks and degraded pore structures. At $n = 0$, there were fewer pores surrounded by a compact framework structure, smoother pore walls, and a pattern of independent pores. After $n = 60$ and 90 cycles, the number of pores increased significantly, the pore walls became extremely irregular, and the pores became mutually connected; in the process, a needle-silk framework developed around the pores, and the pore clusters adopted a sponge-type framework. After $n = 120$ cycles, the number of small pores increased significantly and the pore clusters and framework assumed a rough and loose composition.

Figure 6 shows changes in the pore structure features with increasing fly ash replacement ($n = 120$). It is seen that increasing the replacement roughened the fracture surface structure and increased the number of pores and filaments. Relative to concrete specimens with no fly ash, the specimens with fly ash developed a more unfavorable pore structure and experienced a higher degree of pore structure deterioration.

3.3. Microtopographic Features on Fracture Surface of Fly Ash Concrete after Freezing and Thawing-Creep Deformation. We then analyzed the morphological structures of brittle and tough fractures in concrete specimen fracture surfaces with creep deformation damage following freezing and thawing.

3.3.1. Brittle Fractures. Based on an analysis of the appearance of microfractures in fly ash concrete specimens following freezing and thawing-creep deformation damage, four basic brittle fracture patterns were identified (Figure 7):

River pattern: the weakest parts of multiphase crystals in concrete materials characterized by disordered and extremely nonhomogeneous arrangements are snapped or cut off under tensile stress. Many tiny steps develop on the fracture surfaces of such crystals as a result of their irregular geometrical shapes or surrounding constraints, resulting in the formation of river flower fractures, as shown in Figure 7(a). These fractures have flat forms and demonstrate typical brittle fracture features.

Step pattern: crystals with complicated components can be ruptured, torn, or cut off under external forces, resulting in the formation of step patterns, as shown in Figure 7(b).

Irregular pattern: the weak surfaces of a concrete can generate fractures and damage under external force, resulting in the formation of irregular shapes and patterns, as shown in Figure 7(c). With their intergranular fracture features, these types of fracture are of a typical brittle type.

Semispherical surface pattern: this fracture pattern is rarely observed in rocks. In cases in which the weak interface between a spherical fine aggregate and cement jelling material is tensioned or sheared under an external force, fractures and separation of fine aggregates can occur, leaving a semispherical pattern, as shown in Figure 7(d). In this case, the spherical surface will be smooth and a typical brittle fracture will occur.

3.3.2. Tough Fractures. Tough fractures, which are generated as a result of plastic deformation, have irregular fracture surfaces. Two tough fracture types—dimple and fungling patterns—were identified in the SEM images and then analyzed.

(1) Dimple Pattern. Figure 8(a) shows an SEM image of the topographical features of a dimple fracture surface. On this

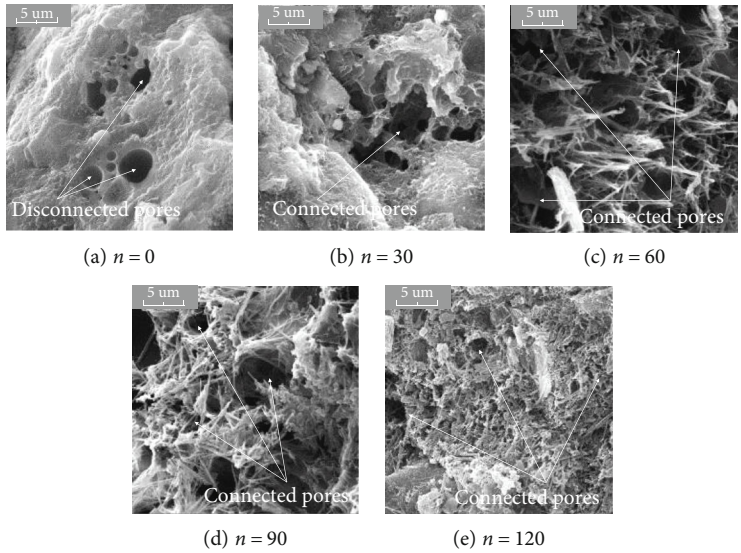

(a) $n = 0$ (b) $n = 30$ (c) $n = 60$

(d) $n = 90$ (e) $n = 120$

Figure 5: Pore characteristics of concrete after increasing numbers freeze-thaw cycles ($m = 35\%$).

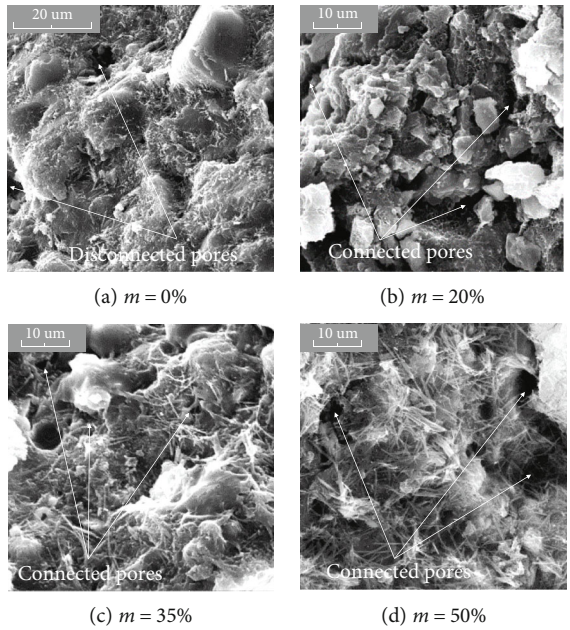

(a) $m = 0\%$ (b) $m = 20\%$

(c) $m = 35\%$ (d) $m = 50\%$

Figure 6: Pore characteristics of concrete mixed with fly ash ($n = 120$).

surface, large numbers of pores in the concrete have nucleated, grown, and deformed plastically, with the resulting structures running through and tearing under the effect of loading, resulting in the formation of dimples.

(2) Fungling Pattern. This topographic feature is widely observed in fly ash concrete specimens after freezing and thawing. Fungling fractures are formed through a mechanism similar to that causing dimples via the tearing of pores as a result of external force. However, fungling patterns are often formed in regions with higher pore densities in which the pore or pore cluster walls are relatively thin, enabling plastic deformation of the pore walls under the effect of tensile stress. The walls are eventually pulled out, forming a fungling pattern (Figure 8(b)).

To further analyze the influence of freezing and thawing on the topographic features of concrete fractures, SEM images of concretes ($m = 35\%$) subjected to increasing numbers of freezing-and-thawing cycles were analyzed (Figure 9). At $n = 0$, (Figure 9(a)), the fractures featured hidden river patterns that were distributed with irregular short and small tearing edges, indicating a change in the concrete damage features from brittle to ductile fractures. After $n = 60, 90,$ and 120 cycles, as shown in Figures 9(c)–9(e), respectively, fungling patterns developed on the fractures (ductile fracture

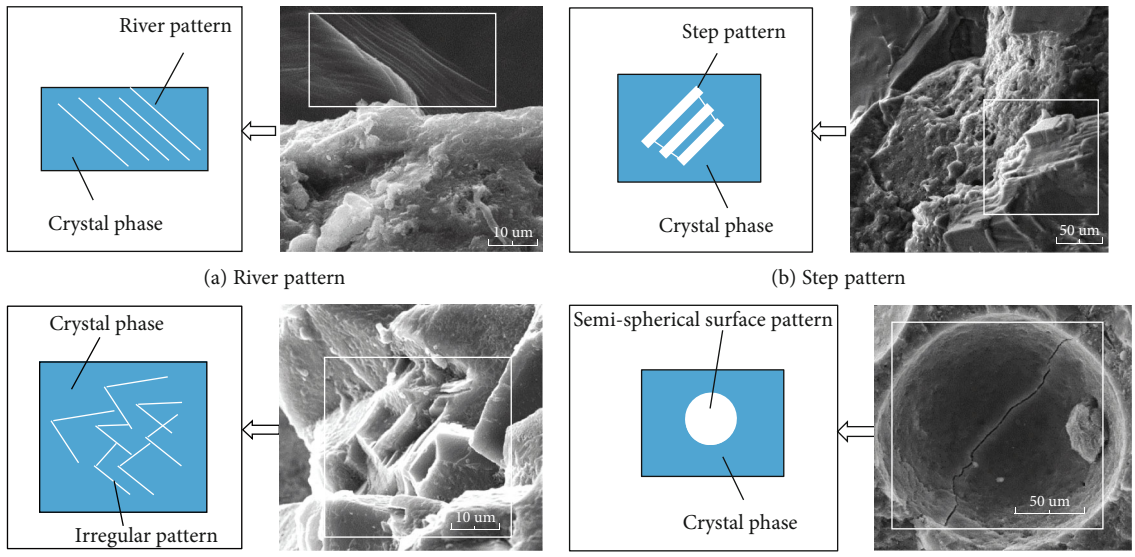

Figure 7: Brittle fracture morphology.

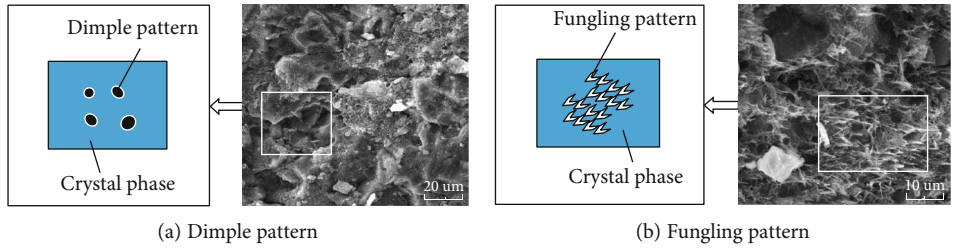

Figure 8: Ductile fracture morphology.

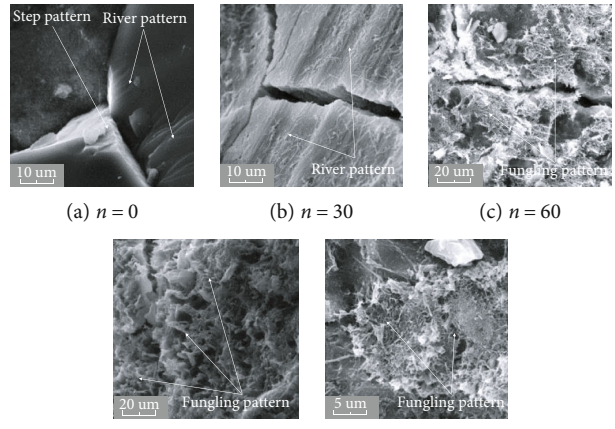

Figure 9: Fracture morphology of concrete after different freeze-thaw cycles ($m = 35\%$).

feature). The fungling patterns became denser as the number of freezing-and-thawing cycles increased.

Figure 10 shows the changes in the fracture topographic features as the amount of fly ash replacement was increased ($n = 120$). At $m = 0\%$ (Figure 10(a)), the intergranular fracturing of the semispherical patterns was uniform. At $m = 20\%$ (Figure 10(b)), large numbers of dimples with plastic fracture features developed on the fractures. At $m = 35$ and 50% (Figures 10(c) and 10(d), respectively), large numbers of fungling patterns developed

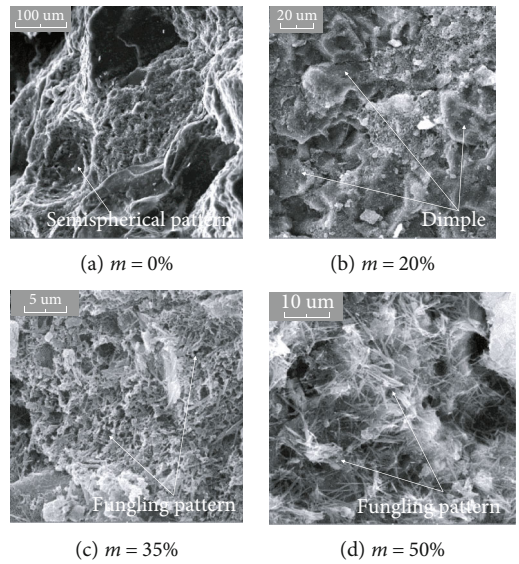

(a) $m = 0\%$ (b) $m = 20\%$

(c) $m = 35\%$ (d) $m = 50\%$

Figure 10: Fracture morphology of concrete mixed with fly ash ($n = 120$).

in the fractures. These results indicate that increasing the fly ash replacement in a concrete will change its postfreezing-and-thawing microfracture features from brittle to ductile.

4. Conclusions

The results of this study suggest that, as the number of freezing-and-thawing cycles increases, the macrofractures of a concrete specimen will evolve from a smooth to an irregular morphology in which there are more cracks on the fractures. In this process, the specimens will be gradually divided into many small regions surrounded by cracks. As the fly ash replacement is increased, the specimen will develop an improved fracture degree.

In our specimens, we identified four types of concrete pore structure—single-pore, disconnected pore clusters, connected pore clusters, and fly ash pores. At a constant fly ash replacement ($m = 35\%$), increasing the number of freezing-and-thawing cycles reduced the number of disconnected pore clusters, while increasing the number of connected clusters produced a needle-silk or flower piece framework around the pores with an enhanced degree of pore structure deterioration. The same results were obtained by increasing the fly ash replacement and subjecting the samples to a constant number of freezing-and-thawing cycles ($n = 120$).

The microtopographic features of concrete fractures are primarily brittle (river, step, stacking, semispherical surface, or irregular patterns) or tough (dimple or fungling patterns). With the fly ash replacement held constant ($m = 35\%$), the concrete fracture features changed from brittle to ductile as the number of freezing-and-thawing cycles increased; the same results were obtained when the fly ash replacement was increased, while the number of freezing-and-thawing cycles remained constant ($n = 120$).

Data Availability

All data, models, and code generated or used during the study appear in the submitted article.

Conflicts of Interest

The authors declare that there is no conflict of interest regarding the publication of this paper.

Acknowledgments

The authors gratefully acknowledge the financial support for this work, provided by the National Natural Science Foundation (52074240, 51974296), the Research project of "333 project" in Jiangsu Province of China (BRA2019236), the Natural Science Research Project of Higher Education of Jiangsu (General Program 16KJB560017, 17KJA560004, 18KJB560019), the Science and Technology Project of the Jiangsu Department of Housing and Urban-Rural Construction (2017ZD163), and the Research Program of Xuzhou Institute of Technology (XKY2018131), the Xuzhou Key Research and Development Program (KC18090, KC20176), and the Science and Technology Project of Xuzhou City (KC18241).

References

[1] Z. Li, H.-X. Liu, Z.-L. Dun, L.-W. Ren, and J.-J. Fang, "Grouting effect on rock fracture using shear and seepage assessment," *Construction and Building Materials*, vol. 142, p. 118131, 2020.

[2] Z. Li, H. Zhou, D.-W. Hu, and C.-Q. Zhang, "Yield criterion for rocklike geomaterials based on strain energy and CMP model," *International Journal of Geomechanics*, vol. 20, no. 3, article 04020013, 2020.

[3] Z. Li, S.-G. Liu, W.-T. Ren, J.-J. Fang, Q.-H. Zhu, and Z.-L. Dun, "Multiscale laboratory study and numerical analysis of water-weakening effect on shale," *Advances in Materials Science and Engineering*, vol. 2020, Article ID 5263431, 14 pages, 2020.

[4] X. Wang, C. Liu, S. Chen, L. Chen, K. Li, and N. Liu, "Impact of coal sector's de-capacity policy on coal price," *Applied Energy*, vol. 256, article 114802, 2020.

[5] Q. Meng, H. Wang, M. Cai, W. Xu, X. Zhuang, and T. Rabczuk, "Three-dimensional mesoscale computational modeling of soil-rock mixtures with concave particles," *Engineering Geology*, vol. 277, p. 105802, 2020.

[6] W.-L. Jin and D.-T. Niu, "The state-of-the-art on durability and life-cycle design theory of engineering structures," *Engineering Mechanics*, vol. 12, pp. 31–33, 2011.

[7] Y. Wang, D.-T. Niu, and Y.-Y. Miao, "Durability of steel fiber reinforced concrete under the combined effects of carbonization and acid rain erosion," *Journal of Building Materials*, vol. 17, pp. 579–585, 2014.

[8] D.-F. Cao, L.-Z. Fu, and Z.-W. Yang, "Experimental study on tensile properties of concrete after freeze-thaw cycles," *Journal of Building Materials*, vol. 5, pp. 48–52, 2012.

[9] Y.-L. Chen, M.-J. Liu, and L.-H. Jiang, "Experimental study on mechanical properties of concrete with cracks after freeze-thaw cycles," *China Civil Engineering Journal*, vol. 44, pp. 230–233, 2011.

[10] H.-Y. Su, J.-Y. Xu, and W.-B. Wu, "Experimental study on the dynamic compressive mechanical properties of concrete at elevated temperature," *Materials and Design*, vol. 56, pp. 579–588, 2014.

[11] Z.-D. Wang, Q. Zeng, L. Wang, Y. Yao, and K.-K. Li, "Corrosion of rebar in concrete under cyclic freeze-thaw and Chloride salt action," *Construction and Building Materials*, vol. 53, pp. 40–47, 2014.

[12] H.-S. Shang, L. Cao, and H.-P. Wang, "Brittle elastic damage constitutive model of plain concrete under biaxial compression after freeze-thaw cycles," *Journal of Jiangsu University (Natural Science Editions)*, vol. 35, pp. 727–731, 2014.

[13] A. M. Firas, J. M. Mechling, and S. Mohamed, "Bond strength of different strengthening systems–concrete elements under freeze–thaw cycles and salt water immersion exposure," *Construction and Building Materials*, vol. 70, pp. 399–409, 2014.

[14] H. Zhang and D.-M. Wei, "A micro fracture model for concrete considering the influence of temperature," *Engineering Mechanics*, vol. 27, pp. 14–20, 2010.

[15] X.-M. Wan, T.-B. Zhang, T.-J. Zhao, C.-B. Jiang, and X.-C. Ren, "Microstructures and chloride permeability of concrete under salt first," *Journal of Building Materials*, vol. 18, pp. 633–639, 2015.

[16] W.-H. Yang, G.-X. Cui, G.-Q. Zhou, Y. Li, X.-D. Chen, and H.-L. Lv, "Fracture mechanism of shaft lining under special strata condition and the technique preventing the shaft from fracturing (part one)," *Journal of Chnia University of Mining and Technology*, vol. 25, no. 4, pp. 1–5, 1996.

[17] L.-F. Dai and J. Tan, "Development and application of the special mine shaft sinking technology to coal mines in China," *Coal Engineering*, vol. 45, no. 12, pp. 9–12, 2013.

[18] Q. Yu, J. Ma, H. Shimada, and T. Sasaoka, "Influence of coal extraction operation on shaft lining stability in eastern Chinese coal mines," *Geotechnical and Geological Engineering*, vol. 32, no. 4, pp. 821–827, 2014.

[19] X.-S. Chen, "Time-space design theory for deep Ice wall of short cylinder," *Chinese Journal of Geotechnical Engineering*, vol. 20, no. 5, pp. 13–16, 1998.

[20] R.-J. Chen, G.-D. Cheng, S.-X. Li, X.-M. Guo, and L.-N. Zhu, "Development and prospect of research on application of artificial ground freezing," *Chinese Journal of Geotechnical Engineering*, vol. 22, no. 1, pp. 40–44, 2000.

[21] T. Wang, F.-T. Yue, Y.-D. Jiang, and T.-Q. Zheng, "Research and practice on forced thaw technology applied to frozen wall of mine shaft," *Journal of China Coal Society*, vol. 35, no. 6, pp. 918–922, 2010.

[22] Z.-S. Yao, H. Cheng, and J.-J. Yang, "The experimental study on high strength reinforced concrete shift lining in deep alluvium," *Journal of China Coal Society*, vol. 29, no. 4, pp. 167–171, 2004.

[23] Z.-S. Yao, "An experimental study on steel fiber reinforced high strength concrete shaft lining in deep alluvium," *Chinese Journal of Rock Mechanics and Engineering*, vol. 24, no. 7, pp. 1253–1258, 2005.

[24] Z.-S. Yao, H. Cheng, and C.-X. Rong, "Experimental study on composite shaft lining of inner steel plate cylinder and high strength reinforced concrete in deep frozen shaft," *Chinese Journal of Rock Mechanics and Engineering*, vol. 27, no. 1, pp. 154–160, 2008.

[25] Z.-S. Yao, H. Cheng, and C.-X. Rong, "Shaft structural design and optimization of deep freezing bedrock shaft in west area," *Journal of China Coal Society*, vol. 35, no. 5, pp. 760–764, 2010.

[26] Q.-X. Zhao, W. Sun, K.-R. Zheng, H.-S. Chen, F.-G. Qin, and J.-Z. Liu, "Influence of fly ash proportion on creep characteristics of high-performance concrete and its mechanism," *Journal of the Chinese Ceramic Society*, vol. 34, pp. 447-448, 2006.

[27] P. Rossi, J. L. Tailhan, and F. L. Maou, "Comparison of concrete creep in tension and in compression: Influence of concrete age at loading and drying conditions," *Cement and Concrete Research*, vol. 51, pp. 78–84, 2013.

[28] N. Ranaivomanana, S. Multon, and A. Turatsinze, "Tensile, compressive and flexural basic creep of concrete at different stress levels," *Cement and Concrete Research*, vol. 52, pp. 1–10, 2013.

[29] C.-H. Zhang, X.-W. Tang, Y.-D. Zhou, and H. Jiang, "State-of-the-art literature review on concrete meso-scale mechanics," *Journal of Hydroelectric Engineering*, vol. 34, pp. 1–18, 2015.

[30] B. Li, H.-G. Yin, X.-B. Mao et al., "Macroscopic and microscopic fracture features of concrete used in coal mine under chlorine salt erosion," *International Journal of Mining Science and Technology*, vol. 26, no. 3, pp. 455–459, 2016.

[31] L.-Y. Zhang, R.-X. Liu, Y. Li, H. G. Yin, L. Song, and B. Li, "Expermental research on damage mechanics properties of concrete with different strength after freeze-thaw cycles," *Journal of Hydraulic Engineering*, vol. S1, pp. 143–146, 2014.

[32] B. Li, L.-Y. Zhang, Y. Li, H.-G. Yin, and R.-X. Liu, "Stepwise loading-unloading creep testing of fly ash concrete and its constitutive model," *Thermal Science*, vol. 23, no. 3, Part A, pp. 1539–1545, 2019.

[33] S.-P. Zhang, M. Deng, J.-H. Wu, and M.-S. Tang, "Effect of pore structure on the frost resistance of concrete," *Journal of Wuhan University of Technology*, vol. 30, pp. 56–59, 2008.